

Effective Elastic Properties of Multilayer Graphene

Yun Hwangbo,¹ Seong-jae Jeon,¹ Young-Woo Son,² and Sungjong Woo^{3,*}

¹Korea Institute of Machinery & Materials, Daejeon 305-343, Republic of Korea

²Korea Institute for Advanced Study, Seoul, Republic of Korea

³Pukyong National University, Pusan, Republic of Korea

(Dated: June 25, 2024)

We present experimental measurements on Young's modulus and Grüneisen parameter of multilayer graphene with varying number of layers using *in situ* bulge tests corroborated by atomic force microscopy and Raman spectroscopy. Due to the experimental challenges posed by the significant disparity between intra- and inter-layer mechanical strengths, measuring conclusive elastic parameters are proven difficult. We analyze the results based on a new theoretical model together with first-principles calculations to elucidate the mechanism of thickness dependent incomplete strain transfer across the layers. Our findings indicate that the experimental elastic constants, which differ from intrinsic computed ones, have unavoidable limitations in reflecting ideal mechanical couplings between layers. Consequently, we propose a new mechanical modulus, free from effects of uncontrollable delamination of layers, derived by combining Grüneisen parameter with Young's modulus.

Multilayered two-dimensional (2D) materials have highly anisotropic elastic behaviors due to their unique atomic structure [1–3]. Single layer is formed by covalent bonds while neighboring layers are bound by van der Waals (vdW) interaction. The vdW interaction, though it is weaker in materials compared with the ionic, covalent and metallic bonds [4], is essential for constructing various multilayered 2D materials [5, 6]. In graphite, the strong sp^2 covalent bond makes a hexagonal lattice while layers glue together by the weak vdW attraction [7].

Owing to anisotropic natures in their structures, many physical properties of layered materials such as electrical, thermal and optical ones change their characteristics from their 2D limit to three-dimensional (3D) bulk ones depending on the number of layers (N_{lay}) [8–10]. Their mechanical properties may also alter accordingly. Based on currently available studies [11–22], the dimensional dependence of mechanical properties of graphene, especially Young's modulus (E), is not thoroughly investigated. When the thickness of multilayer graphene samples increases, all three possibilities for variation of E – increase, decrease or remain unchanged – have been reported [11–22]. Questions such as whether there is any dimensional crossover or transition for mechanical properties, and if there is, what is the critical N_{lay} and which physical parameter dominates, are important and fundamental, but have not been answered conclusively so far.

In this Letter, we explore the elastic behaviors of graphene such as variations of its E and Grüneisen parameter (γ) with increasing its thickness from one to twenty one layers through *in-situ* bulge tests together with simultaneous spectroscopic measurements. We also perform extensive first-principles calculations based on density functional theory (DFT) as well as mechanical model calculations to consider realistic situations beyond simple periodic unitcell geometries for DFT calculations. Our main finding is a sharp dichotomy between measurements and computational results such that calculated

E [23] and γ are independent of N_{lay} while our measured ones substantially decrease with increasing thickness. We found that the origin of such a discrepancy is inevitable experimental overestimation of strains owing to their intrinsic difference between inter- and intra-layer mechanical couplings. We believe that our finding of experimental circumscription in measuring mechanical properties of multilayer graphene would also be unavoidable for other layered materials. Through careful analysis, we propose a new mechanical modulus of $E/\gamma^{3/2}$ to characterize intrinsic mechanical properties of multilayered vdW materials free from uncontrollable interlayer slidings.

We prepare graphene samples with various thickness ranging from single to twenty one layers. Figure 1(a) shows optical images of some graphene samples. To determine N_{lay} precisely, we mainly use optical transmittance [10] and Raman spectroscopy shown in Fig. 1 (b) and (d), respectively [24, 25]. Up to seven layers, Raman spectroscopy determines the number of layers. Optical transmittance data is fit to N_{lay} and extrapolated over seven layers to determine N_{lay} . TEM [26] measurements were also carried out to cross check the thickness.

To measure E and γ , *in-situ* bulge tests are performed along with atomic force microscopy (AFM) as shown in Fig. 1 (c) and Raman spectroscopy in Fig. 1(d). Stress is applied to graphene using pressure difference of P between the atmospheric (P_{atm}) and the vacuum chamber pressure (P_i). In order to avoid delamination of graphene from the substrate, we set P_i to be smaller than P_{atm} . The bulge height of h is measured by a non-contact mode of AFM as shown in Fig. 1(c). Using P and h , stress and strain of deformed graphene samples are obtained from the analytical formula for a typical bulge test shown in Eq. (1). To measure γ , the Raman shift as a function of equibiaxial strain is obtained from the *in-situ* Raman bulge test as shown in Fig. 1(d). The positions of Raman G and $2D$ bands are obtained from Lorentzian fitting for each strain. Here, only the Grüneisen parameter for the

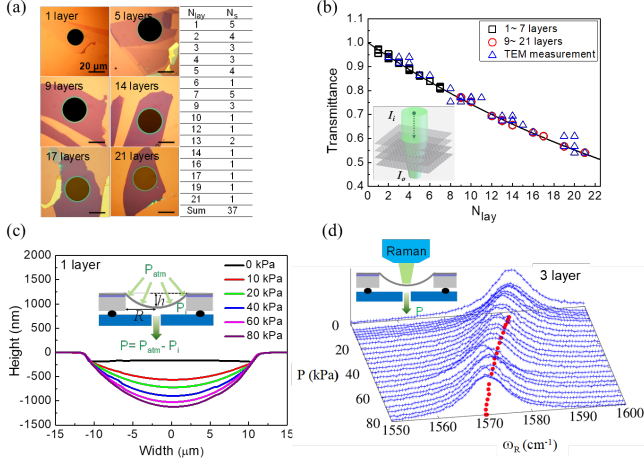


FIG. 1. (a) Graphene with various numbers of layers (N_{lay}) on perforated SiO_2/Si substrate with different numbers of samples (N_s). (b) Optical transmittance as a function of N_{lay} . Up to seven layers, Raman spectroscopy is used to measure N_{lay} and then the transmittance used for $N_{\text{lay}} > 7$. (c) In-situ AFM-bulge test for Young's modulus and (d) in-situ Raman spectra for different pressures to determine Grüneisen parameters. G -peak positions are denoted as red dots.

G band is used to simplify our analysis (see SI for experimental details).

In a bulge test, with the assumption of perfect clamping on the edge, the values of biaxial strain and stress at the center of the bulge are approximately $\epsilon = 2h^2/3R^2$ and $\sigma = PR^2/4ht$ [27] so that Young's modulus can be written as

$$E = (1 - \nu) \frac{\sigma}{\epsilon} = (1 - \nu) \left(\frac{3R^4}{8t} \right) \left(\frac{P}{h^3} \right), \quad (1)$$

where P , h , R , t and ν are applied pressure, the bulge height, radius of the hole, the thickness and the Poisson's ratio of the sample in Fig. 2(a). With dimensionless expressions, $\bar{q} \equiv \frac{PR}{Et}$, $\bar{\sigma} \equiv \frac{\sigma}{E}$, $\bar{h} \equiv \frac{h}{R}$ and $k = \frac{8}{3(1-\nu)}$, Eq. (1) can be rewritten as

$$\bar{q} = k\bar{h}^3, \quad (2)$$

where

$$\bar{\sigma} = \frac{\bar{q}^{\frac{2}{3}}}{2(3(1-\nu))^{\frac{1}{3}}}. \quad (3)$$

In our experiments, the bulge height is measured as a function of applied pressure for various samples with varying N_{lay} . The diameter of the hole for different samples ranges from 20 to 30 μm . We calculate the values of Young's modulus of multilayer graphene depending on N_{lay} using Eq. (1) with inputs from our experimental data and results are plotted in Fig. 3(d). It shows that the experimental Young's modulus decreases substantially as N_{lay} increases. On the other hand, a previous DFT report shows that the Young's modulus of

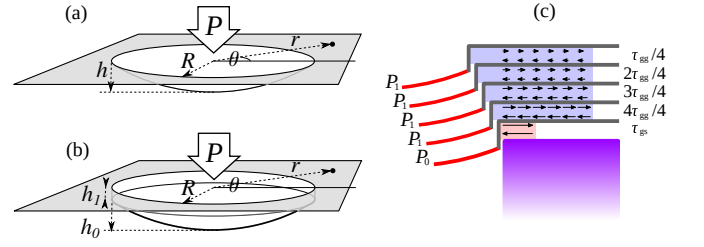


FIG. 2. (a) Schematic picture of bulge test. R is the radius of bulge hole, h is bulge height. (a) is the case of perfect clamping while (b) is when interlayer sliding is taken into account. h_0 is the same as h in (a) while h_1 is the additional height pulled in from the supported region. (c) The cross-sectional view of multilayer graphene on top of SiO_2 (purple block) near the hole edge that shows the distribution of interlayer stresses under pressure.

multilayer graphene is barely dependent on N_{lay} (plotted in Fig. 3(d)) [23]. In this work, we show that the experimental deviation from the DFT result is attributed to the imperfect clamping of the graphene to the substrate as well as the interlayer sliding between graphene layers [7].

With interlayer sliding, interlayer shear strength (τ) or the maximum value of interlayer shear stress is built against the direction of sliding. It is the force that gives a static friction. We use dimensionless interlayer shear strength, $\bar{\tau} \equiv \tau R/Et$. Wang *et al.* estimated the values of τ between graphene and SiO_2 substrate and between graphene and graphene using bulge tests [7]. Hereafter, the former is denoted by τ_{gs} and the latter τ_{gg} . They found that, when the suspended graphene within a hole of the substrate is pressurized, shear stress is built due to interlayer sliding across the supported region outside the hole which is to be balanced against the intralayer stress within the suspended region. Their approach was successful for single and bilayer graphene. The method, however, cannot be applied for more than two layers.

The key to understand the bulge test in the presence of the interlayer sliding lies on proper estimation on a distance how far the sample on the rim around the hole is pulled inward. This additional pulling would give an additional contribution to the bulge height so that the sample would look softer than the case without it. Let us first consider a single layer case with this effect. The equation of equilibrium of graphene in the supported region outside of the hole can be written as

$$\frac{\partial \bar{\sigma}_r}{\partial \rho} + \frac{\bar{\sigma}_r - \bar{\sigma}_\theta}{\rho} + \bar{\tau} = 0, \quad (4)$$

where dimensionless radial distance is defined by $\rho \equiv r/R$. The stress for the region with $\rho < 1$ obtained by Eq. (3) is most valid near the center of the hole. As $\rho \rightarrow 1$ from the inside, azimuthal component of stress becomes very small – no stretch along the circumferential direction – so that the radial component of stress should become roughly double the value of Eq. (3). With conditions for

isotropy and continuity of $\bar{\sigma}_r$ at $r = R$, the solutions are

$$\bar{\sigma}_r = -\frac{2 + \nu}{3} \bar{\tau} \rho + \frac{A}{1 - \nu} - \frac{B}{1 + \nu} \frac{1}{\rho^2}, \quad (5)$$

$$\bar{\sigma}_\theta = -\frac{1 + 2\nu}{3} \bar{\tau} \rho + \frac{A}{1 - \nu} + \frac{B}{1 + \nu} \frac{1}{\rho^2}, \quad (6)$$

where $A = \frac{1}{2} (1 - \nu^2) \bar{\tau} \rho_{\max}$ and $B = -\frac{1}{6} (1 - \nu^2) \bar{\tau} \rho_{\max}^3$. Here, ρ_{\max} is the solution of a cubic equation of x , $\frac{1-\nu}{6} (x-1)^3 + \frac{1-\nu}{2} (x-1)^2 + (x-1) = \zeta [3(1-\nu)]^{-\frac{1}{3}}$ where $\zeta \equiv \bar{q}^{2/3} / \bar{\tau}$. Here, ρ_{\max} represents another boundary condition such that σ_r and σ_θ simultaneously vanishes at $\rho = \rho_{\max}$. Strains can be obtained using $\epsilon_r = \bar{\sigma}_r - \nu \bar{\sigma}_\theta$ and $\epsilon_\theta = \bar{\sigma}_\theta - \nu \bar{\sigma}_r$ (see SI for detailed derivation).

Now, the radial displacement is $\bar{u}_r = \rho \epsilon_\theta$ in an isotropic system, whose value at $\rho = 1$ represents the amount of pulling-in of graphene at the rim of the hole; $\bar{u}_r(\rho = 1) = -\frac{(1-\nu^2)}{6} \bar{\tau} [(\rho_{\max} - 1)^3 + 3(\rho_{\max} - 1)^2]$. As depicted schematically in Fig. 2(b), this pulling-in provides additional contribution to the bulge height, $\bar{h}_1 = -\bar{u}_r(\rho = 1)$, so that the total bulge height becomes $\bar{h} = \bar{h}_0 + \bar{h}_1$, where \bar{h}_0 is from Eq. (2).

In case of perfect clamping, $\bar{\tau} \rightarrow \infty$ and $\zeta \rightarrow 0$ so that $\rho_{\max} \rightarrow 1$ and \bar{h}_1 becomes zero. Then, the relation between \bar{q} and \bar{h}^3 becomes the same as Eq. (2). With

graphene-substrate sliding allowed, i.e., $\bar{h}_1 \neq 0$, the coefficient k in Eq. (2) becomes dependent on $\bar{\tau}$ and ζ ,

$$k_{\bar{\tau}}(\zeta) = \left[\frac{(3(1-\nu))^{\frac{1}{3}}}{2} + \frac{(1-\nu^2)}{6} \left(\frac{\bar{\tau}}{\zeta} \right)^{\frac{1}{2}} f(\rho_{\max}) \right]^{-3} \quad (7)$$

where $f(x) \equiv (x-1)^3 + 3(x-1)^2$. For two limiting cases, $\zeta \ll 1$ and $\zeta \gg 1$ with $\nu = 0.144$ [23], $k_{\bar{\tau}}(\zeta)$ can be approximated as

$$k_{\bar{\tau}}(\zeta) \approx 3.12 \left(1 + \frac{\bar{q}(1+\nu)}{\bar{\tau}} \right)^{-3}, \quad (8)$$

and

$$k_{\bar{\tau}}(\zeta) \approx \frac{1.72}{\bar{q}}, \quad (9)$$

respectively. Recalling that $\zeta = \frac{\bar{q}^{2/3}}{\bar{\tau}}$, $\bar{q} = \frac{PR}{Et}$ and $\bar{\tau} = \frac{\tau R}{Et}$, Eqs. (8) and (9) show that $k_{\bar{\tau}}(\zeta)$ begins to decrease from the perfect clamping case if $P \sim \tau$ and approaches to zero if $P > Et/R$. These two criteria determine the overall shape of the k vs. P graph. For our experiments, the second criteria becomes $Et/R \sim 35$ MPa, with $R \sim 10$ μm , $t = 3.35$ \AA and $E = 1075$ GPa. Our experimental condition which is up to about several tens kPa is not in such an extreme regime but near the first criteria.

For each given pressure, we calculate \bar{h} and corresponding k using Eq. (7). Figure 3(a) shows k as a function of P for two different values of τ such as $\tau_{\text{gg}} = 40$ kPa and $\tau_{\text{gs}} = 1640$ kPa [7]. The value of k begins to decrease at different pressures corresponding to each τ value, while k suppresses to zero over the same pressure, Et/R . The hatched area is our experimental pressure range. Because of the interlayer sliding effect considered in Eq. (7), \bar{q} is not simply proportional to \bar{h}^3 . Figure 3(b) shows the amount of deviation from the linear correlation (dotted line) upto the hatched area in Fig. 3(a).

Let us consider multilayer cases for which shear stress should be distributed properly across the layers with the maximal value limited by τ . Figure 2(c) shows the configuration of the distribution of interlayer shear stresses; the difference between neighboring shear stresses should be balanced with the intralayer stress of the strained graphene in the suspended region. In order for all the upper layers except the bottom layer move harmonically together, differences between stresses on neighboring layers should be the same so that the interlayer shear stress must increase monotonically from the top to lower layers. For example, in the case of five-layer graphene on a substrate, the distribution of interlayer shear stress should be like Fig. 2(c). All the layers except the bottom layer experience the same net radial stress of $\tau_{\text{gg}}/4$. It allows each layer's ρ_{\max} and corresponding \bar{h} to be all simultaneously the same if the total pressure is equally distributed except the bottom layer. Bottom layer experiences a net

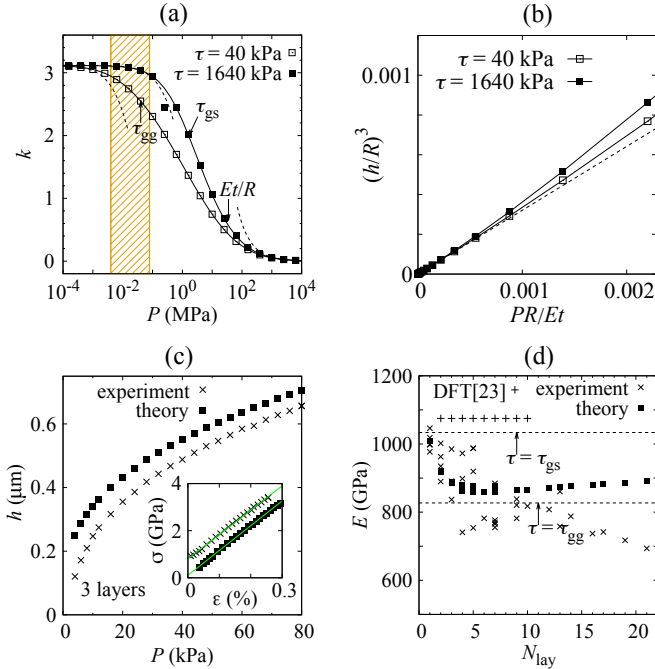


FIG. 3. (a) $k_{\bar{\tau}}(\zeta)$ as a function of P for $\tau = \tau_{\text{gg}}$ and τ_{gs} . (b) Nonlinear behavior of \bar{h}^3 with respect to \bar{q} depending on τ . Dashed line is for a perfect clamping case. (c) h as a function of P . Inset represents σ vs. ϵ curve to get Young's modulus. (d) Young's modulus (E) as a function of N_{lay} . Dashed lines are the theoretical boundaries for E of single layer on a substrate and graphene.

stress of $\tau_{gs} - \tau_{gg}$. Total pressure of P is distributed across the layers such that $P = (N_{\text{lay}} - 1)P_u + P_b$. Here, the ratio between P_u and P_b is determined to make the bulge heights of the layers to have the same value of h . The bulge height for the i -th layer for a given pressure of P_i is calculated using the same procedure as in the single layer case and the subscripts ‘u’ and ‘b’ represent the upper and bottom layers, respectively.

We first calculate h based on the theoretical model discussed so far in case of constant Young’s modulus of graphene regardless of N_{lay} as was obtained from DFT results [23]. Figure 3(c) compares calculated h with varying P for trilayer graphene with experimental results. The inset shows corresponding σ vs. ϵ . We note that a constant offset for the measured height from the model calculation do not affect their ratio or the computed Young’s modulus seriously. Let us call this Young’s modulus obtained with a simple ratio of $(1 - \nu)\frac{\sigma}{\epsilon}$ as ‘apparent Young’s modulus’ or E_{ap} . Solid squares in Fig. 3(d) are the theoretical estimation of E_{ap} using our sample geometries, while the crosses are directly from the experiments. One can see that the theoretical E_{ap} decreases as N_{lay} increases and saturates around $N_{\text{lay}} \simeq 10$ and that our model calculations and measurements match pretty well. So, we may consider ten layers as a critical thickness for mechanical crossover from 2D to 3D characteristics. However, for samples thicker than ten layers, the both deviate each other significantly.

Before discussing the serious discrepancies for cases with $N_{\text{lay}} > 10$, it is worthwhile to compare E_{ap} for multilayers with one for single layer. As shown in Eq. (2), E_{ap} is proportional to k , reflecting effects from substrates. So, E_{ap} decreases to 1034 GPa from its intrinsic 1075 GPa for graphene on SiO_2 substrate and to 827 GPa for graphene on graphene. The overall E_{ap} is areal average so that, as N_{lay} increases, the value approaches to that for graphene on graphene. In Fig. 3(d), E_{ap} for the case with $\tau = \tau_{gs}$ and for the case with $\tau = \tau_{gg}$ are drawn with dashed lines. As discussed, E_{ap} begins with the value for $\tau = \tau_{gs}$ and approaches to one for $\tau = \tau_{gg}$ as N_{lay} increases.

As shown in Fig. 3(d), our estimated E for cases of $N_{\text{lay}} > 10$ deviates from the experimental results, for which we suspect two major sources. One is a formation of wrinkles [20, 22] and the other is delamination of layers. Because of $\bar{u}_r = \rho\epsilon\theta$, isotropic pull of graphene toward the center of the hole causes azimuthal compression, possibly forming wrinkles along the radial direction especially near the edge of the hole where pressurized graphene is structurally unstable due to bending and the instability increases with thickness. Such wrinkles practically reduce intrinsic E under compression along the circumferential direction so that the shape of Fig. 3(a) changes by shifting one of the pressure criteria, Et/R , toward lower P . This, together with the reduction of τ_{gs} due to delamination, further reduces k within our pres-

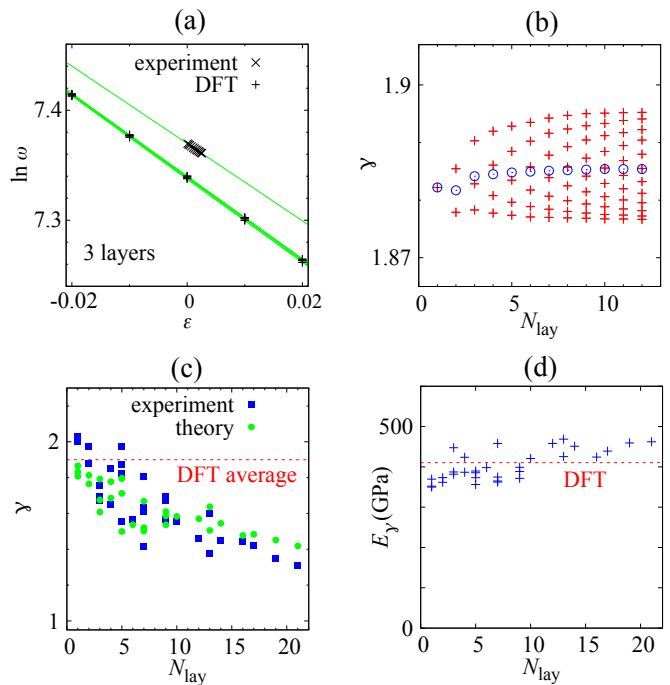


FIG. 4. (a) $\ln \omega$ vs. ϵ plots from DFT calculation and from experiment for phonon frequencies corresponding to Raman G peak for graphene with three layers. There are six modes. Green lines shows linear fitting curves. (b) Grüneisen parameters for varying number of layers from DFT calculations. (c) Grüneisen parameters for varying number of layers (blue solid rectangles). Green solid circles represent γ corrected from the DFT result using Young’s modulus. (d) Elastic Grüneisen parameter (E_γ) from our experiment for different number of layers. Red dashed line shows DFT prediction.

sure range as well as E_{ap} .

To further consider the wrinkle and delamination effects, we first estimate N_{lay} -dependent γ using DFT method [28]. Detailed computational parameters are in Supplementary Information. For each number of layers, phonon frequencies of ω_G corresponding to the Raman G peak are calculated for isotropic strains of ϵ increasing from -0.02 to 0.02 . Using $\gamma = -\partial \ln \omega_G / \partial \epsilon$ [29, 30] (an example for trilayer is shown in Fig. 4(a)), we obtain γ for doubly degenerate $2N_{\text{lay}}$ modes [31–33] of multilayer graphene with N_{lay} [Fig. 4(b)]. We note that the splitting is about one percent of the average values. For $N_{\text{lay}} = 1$, our DFT result agrees with a previous report [33]. In Fig. 4(c), the measured Grüneisen parameters from Raman spectrum are shown to decrease as the number of layers increases in contrast to the constancy of averaged γ from our DFT calculation. We find that this discrepancy can also be attributed to the strain overestimation like E_{ap} .

Let $\bar{\epsilon}$ and $\bar{\sigma}$ be the intrinsic or ideal values of strain and stress averaged over the layers. The averaged strain $\bar{\epsilon}$ should be determined by h_0 instead of h such that $\bar{\epsilon} = (2/3)(h_0/R)^2$, although h_0 cannot be extracted from

experiment directly. Since the intrinsic Young's modulus of $\tilde{E} = (1 - \nu)(3R^4/8t)(P/h_0^3) = 1075$ GPa is independent of N_{lay} [23], $\tilde{\epsilon}$ can be estimated from ϵ using the ratio of measured $E = (1 - \nu)(3R^4/8t)(P/h^3)$ such that

$$\tilde{\epsilon} = \frac{2}{3} \left(\frac{h}{R} \right)^2 \left(\frac{h_0}{h} \right)^2 = \epsilon \left(\frac{h_0}{h} \right)^2 = \epsilon \left(\frac{E}{\tilde{E}} \right)^{2/3}. \quad (10)$$

This formula shows a quantitative scale for the overestimated ϵ using the measured (hence, underestimated) E . The same procedure for intrinsic Grüneisen parameter of $\tilde{\gamma}$ that is also independent of N_{lay} results in

$$\gamma = \frac{1}{\omega} \frac{\partial \omega}{\partial \epsilon} = \frac{\tilde{\epsilon}}{\epsilon} \frac{1}{\omega} \frac{\partial \omega}{\partial \tilde{\epsilon}} = \left(\frac{E}{\tilde{E}} \right)^{2/3} \tilde{\gamma}. \quad (11)$$

Here, we note that the measured γ is underestimated by the same factor for underestimated strain in Eq. (10). A prefactor in Eq. (11) can be used to rescale our constant Grüneisen parameter obtained from DFT calculations as a function of N_{lay} and then resulting γ 's show a good agreement with our measurements as shown in Fig. 4(d).

Considering consequences from incomplete strain transfer or delamination behaviors discussed so far, we propose a new mechanical constant coined as *elastic Grüneisen modulus*, $E_\gamma \equiv E/\gamma^{3/2}$, which is robust against the inevitable experimental underestimation of strain in vdW materials. In Fig. 4(d), E_γ 's for our experiment are nearly independent of N_{lay} and match well with the constant DFT result, thus reflecting intrinsic mechanical properties of layered materials.

In conclusion, we have measured critical elastic properties of multilayer graphene such as Young's modulus and Grüneisen parameter and analyzed them carefully by including shear sliding between layers. Unlike constant intrinsic values for those parameters from *ab initio* calculations, our measured values show strong thickness dependent characteristics, of which origins we attributed to the unavoidable layer slidings. We further propose a new material constant of elastic Grüneisen modulus that is experimentally robust against interlayer shear effects. Considering that similar mechanical properties are shared by almost all vdW materials [23, 34–37], we believe that our new mechanical parameter will be of importance in extracting intrinsic mechanical properties from experiments.

Y.H. was supported by the Technology Innovation Program (20011317) funded by the Ministry of Trade, Industry & Energy (MOTIE, Korea) and the internal research program of the Korea Institute of Machinery and Materials (NK248C). Y.-W.S. was supported by KIAS individual Grant (No. CG031509). S.W. was partially supported by the National Research Foundation of Korea (NRF) grant funded by the Korea government (MSIT) (RS-2023-00278511). Computations were supported by CAC of KIAS.

* Email: physwoo@gmail.com

- [1] K. S. Novoselov, A. Mishchenko, A. Carvalho, and A. H. C. Neto, 2d materials and van der waals heterostructures, *Science* **353**, aac9439 (2016).
- [2] S. Manzeli, D. Ovchinnikov, D. Pasquier, O. V. Yazyev, and A. Kis, 2d transition metal dichalcogenides, *Nat. Rev. Mater.* **2**, 17033 (2017).
- [3] D. G. Papageorgiou, I. A. Kinloch, and R. J. Young, Mechanical properties of graphene and graphene-based nanocomposites, *Prog. Mater. Sci.* **90**, 75 (2017).
- [4] W. Callister and D. Rethwisch, *Materials Science and Engineering: An Introduction, 8th Edition* (Wiley, 2009).
- [5] I. V. Geim, A. K. and Grigorieva, Van der Waals heterostructures, *Nature* **499**, 419 (2013).
- [6] J. M. Hamm and O. Hess, Two two-dimensional materials are better than one, *Science* **340**, 1298 (2013).
- [7] G. Wang, Z. Dai, Y. Wang, P. Tan, L. Liu, Z. Xu, Y. Wei, R. Huang, and Z. Zhang, Measuring interlayer shear stress in bilayer graphene, *Phys. Rev. Lett.* **119**, 036101 (2017).
- [8] B. Partoens and F. M. Peeters, From graphene to graphite: Electronic structure around the K point, *Phys. Rev. B* **74**, 075404 (2006).
- [9] D. Kim, Y. Hwangbo, L. Zhu, A. E. Mag-Isa, K.-S. Kim, and J.-H. Kim, Dimensional dependence of phonon transport in freestanding atomic layer systems, *Nanoscale* **5**, 11870 (2013).
- [10] Y. Hwangbo, C.-K. Lee, A. E. Mag-Isa, J.-W. Jang, H.-J. Lee, S.-B. Lee, S.-S. Kim, and J.-H. Kim, Interlayer non-coupled optical properties for determining the number of layers in arbitrarily stacked multilayer graphenes, *Carbon* **77**, 454 (2014).
- [11] O. L. Blakslee, D. G. Proctor, E. J. Seldin, G. B. Spence, and T. Weng, Elastic Constants of Compression-Annealed Pyrolytic Graphite, *J. Appl. Phys.* **41**, 3373 (1970).
- [12] B. WenXing, Z. ChangChun, and C. WanZhao, Simulation of Young's modulus of single-walled carbon nanotubes by molecular dynamics, *Physica B: Condensed Matter* **352**, 156 (2004).
- [13] Bending modes, elastic constants and mechanical stability of graphitic systems, *Carbon* **49**, 62 (2011).
- [14] Y. Zhang and C. Pan, Measurements of mechanical properties and number of layers of graphene from nano-indentation, *Diamond Relat. Mater.* **24**, 1 (2012).
- [15] Y. Zhang and Y. Gu, Mechanical properties of graphene: Effects of layer number, temperature and isotope, *Comput. Mater. Sci.* **71**, 197 (2013).
- [16] J.-U. Lee, D. Yoon, and H. Cheong, Estimation of Young's Modulus of Graphene by Raman Spectroscopy, *Nano Lett.* **12**, 4444 (2012), PMID: 22866776.
- [17] M. Annamalai, S. Mathew, M. Jamali, D. Zhan, and M. Palaniapan, Elastic and nonlinear response of nanomechanical graphene devices, *J. Micromech. Microeng.* **22**, 105024 (2012).
- [18] B. Mortazavi, Y. Rémond, S. Ahzi, and V. Toniazzo, Thickness and chirality effects on tensile behavior of few-layer graphene by molecular dynamics simulations, *Comput. Mater. Sci.* **53**, 298 (2012).
- [19] L. Xiang, S. Y. Ma, F. Wang, and K. Zhang, Nanoin-

- dentation models and Young's modulus of few-layer graphene: a molecular dynamics simulation study, *J. Phys. D: Appl. Phys.* **48**, 395305 (2015).
- [20] J. Han, S. Ryu, D.-K. Kim, W. Woo, and D. Sohn, Effect of interlayer sliding on the estimation of elastic modulus of multilayer graphene in nanoindentation simulation, *EPL* **114**, 68001 (2016).
- [21] G. Wang, Z. Dai, J. Xiao, S. Feng, C. Weng, L. Liu, Z. Xu, R. Huang, and Z. Zhang, Bending of Multilayer van der Waals Materials, *Phys. Rev. Lett.* **123**, 116101 (2019).
- [22] T. Zhong, J. Li, and K. Zhang, A molecular dynamics study of Young's modulus of multilayer graphene, *J. Appl. Phys.* **125**, 175110 (2019).
- [23] S. Woo, H. C. Park, and Y.-W. Son, Poisson's ratio in layered two-dimensional crystals, *Phys. Rev. B* **93**, 075420 (2016).
- [24] A. C. Ferrari, J. C. Meyer, V. Scardaci, C. Casiraghi, M. Lazzeri, F. Mauri, S. Piscanec, D. Jiang, K. S. Novoselov, S. Roth, and A. K. Geim, Raman spectrum of graphene and graphene layers, *Phys. Rev. Lett.* **97**, 187401 (2006).
- [25] Y. Hao, Y. Wang, L. Wang, Z. Ni, Z. Wang, R. Wang, C. K. Koo, Z. Shen, and J. T. L. Thong, Probing Layer Number and Stacking Order of Few-Layer Graphene by Raman Spectroscopy, *Small* **6**, 195 (2010).
- [26] J. Ping and M. S. Fuhrer, Layer number and stacking sequence imaging of few-layer graphene by transmission electron microscopy, *Nano Lett.* **12**, 4635 (2012).
- [27] M. K. Small and W. D. Nix, Analysis of the accuracy of the bulge test in determining the mechanical properties of thin films, *J. Mater. Res.* **7**, 1553 (1992).
- [28] P. Giannozzi, S. Baroni, N. Bonini, M. Calandra, R. Car, C. Cavazzoni, D. Ceresoli, G. L. Chiarotti, M. Cococcioni, I. Dabo, A. D. Corso, S. de Gironcoli, S. Fabris, G. Fratesi, R. Gebauer, U. Gerstmann, C. Gougoussi, A. Kokalj, M. Lazzeri, L. Martin-Samos, N. Marzari, F. Mauri, R. Mazzarello, S. Paolini, A. Pasquarello, L. Paulatto, C. Sbraccia, S. Scandolo, G. Sclauzero, A. P. Seitsonen, A. Smogunov, P. Umari, and R. M. Wentzcovitch, QUANTUM ESPRESSO: a modular and open-source software project for quantum simulations of materials, *J. Phys. Condens. Matter* **21**, 395502 (2009).
- [29] N. Mounet and N. Marzari, First-principles determination of the structural, vibrational and thermodynamic properties of diamond, graphite, and derivatives, *Phys. Rev. B* **71**, 205214 (2005).
- [30] L.-F. Huang, X.-Z. Lu, E. Tennesen, and J. M. Rondinelli, An efficient ab-initio quasiharmonic approach for the thermodynamics of solids, *Comput. Mater. Sci.* **120**, 84 (2016).
- [31] T. M. G. Mohiuddin, A. Lombardo, R. R. Nair, A. Bonetti, G. Savini, R. Jalil, N. Bonini, D. M. Basko, C. Galiotis, N. Marzari, K. S. Novoselov, A. K. Geim, and A. C. Ferrari, Uniaxial strain in graphene by Raman spectroscopy: *G* peak splitting, Grüneisen parameters, and sample orientation, *Phys. Rev. B* **79**, 205433 (2009).
- [32] Y. C. Cheng, Z. Y. Zhu, G. S. Huang, and U. Schwingenschlögl, Grüneisen parameter of the *G* mode of strained monolayer graphene, *Phys. Rev. B* **83**, 115449 (2011).
- [33] C. Androulidakis, E. N. Koukaras, J. Parthenios, G. Kalosakas, K. Papagelis, and C. Galiotis, Graphene flakes under controlled biaxial deformation, *Sci. Rep.* **5**, 18219 (2015).
- [34] A. Falin, Q. Cai, E. J. Santos, D. Scullion, D. Qian, R. Zhang, Z. Yang, S. Huang, K. Watanabe, T. Taniguchi, M. R. Barnett, Y. Chen, R. S. Ruoff, and L. H. Li, Mechanical properties of atomically thin boron nitride and the role of interlayer interactions, *Nat. Comm.* **8**, 15815 (2017).
- [35] K. Liu, Q. Yan, M. E. Chen, W. Fan, Y. Sun, J. Suh, D. Fu, S. Lee, J. Zhou, S. Tongay, J. Ji, J. B. Neaton, and J. Wu, Elastic properties of chemical-vapor-deposited monolayer mos₂, ws₂, and their bilayer heterostructures, *Nano Letters* **14**, 5097 (2014).
- [36] S. Bertolazzi, J. Brivio, and A. Kis, Stretching and breaking of ultrathin mos₂, *ACS Nano* **5**, 9703 (2011), PMID: 22087740, <https://doi.org/10.1021/nn203879f>.
- [37] H. Conley, B. Wang, J. I. Ziegler, R. F. Haglund, S. T. Pantelides, and K. I. Bolotin, Bandgap engineering of strained monolayer and bilayer mos₂, *Nano Letters* **13**, 3626 (2013).